

some. Similar to nucleic acid-templated protein libraries, DNA-templated synthetic libraries, in principle, can be selected for desired properties such as target binding affinity or specificity (10).

To test this possibility, we subjected a minute quantity (100 fmol) of the 65-member DNA-templated macrocyclic fumaramide library to an in vitro selection for binding carbonic anhydrase, a well-studied protein (17). Carbonic anhydrase was immobilized by reaction with *N*-hydroxysuccinimide ester-linked agarose beads, combined with 100 fmol of the 65-member macrocyclic fumaramide library, and washed with buffer. Bound molecules were eluted and subjected to a second iteration of the selection. The DNA templates encoding macrocycles surviving each round of selection were amplified by PCR and digested with the restriction endonuclease *Nla*III. The 65th template (1e) uniquely contains a 5'-CATG-3' sequence in the coding region of the phenyl sulfonamide building block that is cleaved by *Nla*III (Fig. 3B).

Before selection for binding to carbonic anhydrase, *Nla*III digestion reveals that the templates from the macrocycle library do not contain a noticeable representation of template 1e, as expected because the library consists predominantly of other templates. Each selection for binding to carbonic anhydrase successively enriches the template pool for the sequence in 1e, such that after two selections the pool predominantly contains the sequence encoding the phenyl sulfonamide-containing macrocycle (8e) (Fig. 4D). We therefore conclude that a single member of the 65-member DNA-templated macrocycle library was efficiently selected for carbonic anhydrase binding activity.

Macrocycles of the general structure 8 are promising compounds for perturbing the activity of biologically important proteases (18) because of their partial peptidic and conformationally constrained nature. In addition, the electrophilic fumaramide group can capture proximal nucleophiles (Figs. 2C and 4D) such as those present in protease active sites. On the basis of the above findings, efforts to generate and select DNA-templated synthetic libraries of high complexity and structural diversity are under way in our laboratory.

References and Notes

- D. S. Wilson, J. W. Szostak, *Annu. Rev. Biochem.* **68**, 611 (1999).
- H. Lin, V. W. Cornish, *Angew. Chem. Int. Ed. Engl.* **41**, 4402 (2002).
- G. F. Joyce, *Annu. Rev. Biochem.* **73**, 791 (2004).
- S. V. Taylor, P. Kast, D. Hilvert, *Angew. Chem. Int. Ed. Engl.* **40**, 3310 (2001).
- Z. J. Gartner, D. R. Liu, *J. Am. Chem. Soc.* **123**, 6961 (2001).
- Z. J. Gartner, M. W. Kanan, D. R. Liu, *Angew. Chem. Int. Ed. Engl.* **41**, 1796 (2002).
- Z. J. Gartner, R. Grubina, C. T. Calderone, D. R. Liu, *Angew. Chem. Int. Ed. Engl.* **42**, 1370 (2003).
- Z. J. Gartner, M. W. Kanan, D. R. Liu, *J. Am. Chem. Soc.* **124**, 10304 (2002).
- C. T. Calderone, J. W. Puckett, Z. J. Gartner, D. R. Liu, *Angew. Chem. Int. Ed. Engl.* **41**, 4104 (2002).
- J. B. Doyon, T. M. Snyder, D. R. Liu, *J. Am. Chem. Soc.* **125**, 12372 (2003).
- R. B. Woodward *et al.*, *J. Am. Chem. Soc.* **103**, 3210 (1981).
- C.-J. Li, T.-H. Chan, *Organic Reactions in Aqueous Media* (Wiley, New York, 1997).
- Synthesis and characterization details are available on Science Online.
- B. E. Maryanoff, A. B. Reitz, *Chem. Rev.* **89**, 863 (1989).
- A. Jain, G. M. Whitesides, R. S. Alexander, D. W. Christianson, *J. Med. Chem.* **37**, 2100 (1994).
- D. R. Halpin, P. B. Harbury, *PLoS Biol.* **2**, E174 (2004).
- B. C. Tripp, K. Smith, J. G. Ferry, *J. Biol. Chem.* **276**, 48615 (2001).
- D. Lamarre *et al.*, *Nature* **426**, 186 (2003).
- Supported by NIH (National Institute of General Medical Sciences R01GM065865), the Office of Naval Research (N00014-03-1-0749), the Arnold and Mabel Beckman

Foundation, the Searle Scholars Foundation (00-C-101), and the Alfred P. Sloan Foundation (BR-4141). Z.J.G. is a Bristol-Myers Squibb Graduate Research Fellow. B.N.T. and T.M.S. are NSF Graduate Research Fellows. J.B.D. is a National Defense Science and Engineering Graduate Research Fellow. We are grateful to the Bauer Center for Genomics Research for MALDI-TOF mass spectrometric analyses, G. Verdine for LC-MS instrument access, and DNA Software for assistance with codon screening. The rights to commercial development of DNA-templated synthesis have been licensed to Ensemble Discovery, a company for which D.R.L. is a consultant and shareholder.

Supporting Online Material

www.sciencemag.org/cgi/content/full/1102629/DC1
Materials and Methods
Figs. S1 to S5

12 July 2004; accepted 4 August 2004

Published online 19 August 2004;

10.1126/science.1102629

Include this information when citing this paper.

Hydrophobic Collapse in Multidomain Protein Folding

Ruhong Zhou,^{1,2*} Xuhui Huang,² Claudio J. Margulis,²
Bruce J. Berne^{1,2*}

We performed molecular dynamics simulations of the collapse of a two-domain protein, the BphC enzyme, into a globular structure to examine how water molecules mediate hydrophobic collapse of proteins. In the interdomain region, liquid water persists with a density 10 to 15% lower than in the bulk, even at small domain separations. Water depletion and hydrophobic collapse occur on a nanosecond time scale, which is two orders of magnitude slower than that found in the collapse of idealized paraffin-like plates. When the electrostatic protein-water forces are turned off, a dewetting transition occurs in the interdomain region and the collapse speeds up by more than an order of magnitude. When attractive van der Waals forces are turned off as well, the dewetting in the interdomain region is more profound, and the collapse is even faster.

In the folding of globular proteins, it is often useful to picture the hydrophobic residues as being driven together by the action of water, in much the same way as droplets of oil would be driven together in water (1–4), but the presence of both a polar backbone and polar hydrophilic side chains complicates this picture. Most of our current understanding of hydrophobic collapse springs from studies on simple solutes (1–3, 5–18) or of model hydrophobic chains (19–22). The role of the hydrophobic interaction in the folding of peptide chains in water is unfortunately a complex problem. We have chosen to study a structurally simpler problem, the collapse of two-domain proteins, where the starting point is the already folded domains.

In a two-domain protein folding, we can probe the hydrophobic collapse and possible

dewetting in the interdomain region when the two complementary domain surfaces (largely hydrophobic) approach each other. The relative stability of each individual domain and the comparable surface area of the interfacial region also make two-domain protein folding somewhat comparable to the previously studied collapse of idealized paraffin-like plates (3). Furthermore, by turning off various portions of the protein-water interaction, we can better understand the important features of collapse present in the case of proteins, but perhaps not in the collapse of paraffin-like plates or the aggregation of oil droplets.

We simulated, by molecular dynamics (MD), the hydrophobic interaction between the domains of a two-domain protein, the BphC enzyme (1dhy), which functions in degrading toxic polychlorinated biphenyls. One focus is on how the water molecules behave in the interdomain region when the multidomain protein folds (or collapses) into its final shape, after each individual domain has been formed, and how this behavior changes in response to changes in the protein-water interaction. The MD simulations were carried out with an all-atom model of both the

¹Computational Biology Center, IBM Thomas J. Watson Research Center, 1101 Kitchawan Road, Yorktown Heights, NY 10598, USA. ²Department of Chemistry, Columbia University, New York, NY 10027, USA.

*To whom correspondence should be addressed. E-mail: ruhongz@us.ibm.com (R.Z.); berne@chem.columbia.edu (B.J.B.)

protein and water. We then omitted various components of the protein-water interaction potential in further simulations to better understand the solvent-solute response.

The two-domain protein, BphC enzyme of KKS102 (1dhy.pdb) (Fig. 1), was selected on the basis of a recent study of the spatial hydrophobicity profiling (23) on all multidomain proteins in the Protein Data Bank (PDB). The hydrophobicity profiling analysis shows that this two-domain protein has large hydrophobic surface areas on the domain boundary, and it is one of the best such proteins in terms of the first-order hydrophobic moment or hydrophobic dipole reorientation (23). The BphC enzyme is an oligomeric enzyme made up of eight identical subunits, each with 292 amino acid residues. Each subunit consists of two domains: domain 1 (residues 1 to 135) and domain 2 (residues 136 to 292). In the current study, only one subunit (1dhy.pdb) is included, and we refer to it as a two-domain protein. The focus is on the interdomain region of the protein during folding; the details of the simulation are given in (24–27).

For each configuration, three different types of simulations were performed: (i) a “dewetting” simulation started with wet initial conditions (water molecules in the interdomain gap region), and with protein atoms constrained but water and ions free to move; (ii) a “wetting” simulation started with dry initial condition (no water molecules in the interdomain gap), and with protein constrained but water and ions free to move; and (iii) a “folding” simulation, i.e., normal folding simulation with everything flexible. In both the dewetting and wetting simulations, the protein atoms are constrained with a harmonic potential with a force constant of $1000 \text{ kJ mol}^{-1} \text{ \AA}^{-2}$.

For the wetting simulation, the water molecules between the two domains are removed after equilibration with a simple criterion, $d_1 + d_2 \leq D + \delta$, where d_1 and d_2 are the distances of a water oxygen atom to each of the two-domain boundary surface atoms, respectively; D is the domain displacement distance defined in (24); and δ is set equal to 2.5 \AA to account for the average sum of two surface-atom radii. This approach allows us to estimate the gap volume as the number of removed water molecules divided by the bulk water number density. Knowing this volume, we can then estimate the water density in this gap as a function of time by counting the number of molecules inside the gap.

For all of the above simulations, at each gap distance D , 5-ns constant pressure and temperature (NPT) runs are performed for data collection. Simulations are done for the full protein-water interaction and full domain-domain interaction and for a variety of cases where electrostatic and van der

Waals attractive parts (r^{-6} term) of the protein-water and domain-domain interactions were turned on or off, as defined below.

Each trajectory from the 5-ns NPT runs for various gap distances D were analyzed in detail. The snapshots from one such dewetting simulation with an initial interdomain gap distance (28) of 4 \AA are shown in Fig. 2A (top). The number of water molecules inside the interdomain region decreases slowly with time but never approaches zero as in the case of idealized paraffin-like plates (3). It instead converges to a roughly constant number after about 500 ps. The water density decreased from 1.00 g cm^{-3} to about $0.86 \pm 0.04 \text{ g cm}^{-3}$ in about 500 ps for $D = 4 \text{ \AA}$ (Fig. 2A, bottom). Even for very small gap distances, such as 2.5 \AA , which can barely contain one layer of water molecules inside the interdomain region, no complete dewetting, or strong dewetting transition (SDT), was observed. For larger gap distances, as expected, dewetting was not observed, and the water density inside the gap region approached 1.0 g cm^{-3} for the gap distances $D > 6.0 \text{ \AA}$.

Snapshots from the wetting simulation started from the dry initial condition, again with the interdomain gap distance of $D = 4 \text{ \AA}$

(Fig. 2A, middle), show that the number of water molecules inside the interdomain gap increases very quickly in the first few tens of picoseconds and then slowly increases until it converges after about 400 to 500 ps. The final number of the water molecules inside the gap, and thus the water density, agrees very well with the dewetting simulation above, as shown in Fig. 2A (bottom). The converged water density (29) is about 14% lower than the bulk density. Thus, no hysteresis is observed: It appears that thermodynamic equilibrium has been achieved in both simulations after about 500 ps. Because there are eight Na^+ ions in the simulation (to neutralize the system), it is interesting to see if they played a role in the water depletion as a result of osmotic effects. We added 20 more Na^+ and 20 Cl^- ($\sim 0.15 \text{ M}$) in the simulation and found no meaningful change in the water density in the interdomain gap; thus, it seems that the water depletion is mainly due to the hydrophobic effect, not to an osmotic effect.

To see whether there is local water depletion in the neighborhood of the hydrophobic surfaces of the isolated domains of BphC, as would be expected from recent work on the equivalent of “oil droplets,” where this deple-

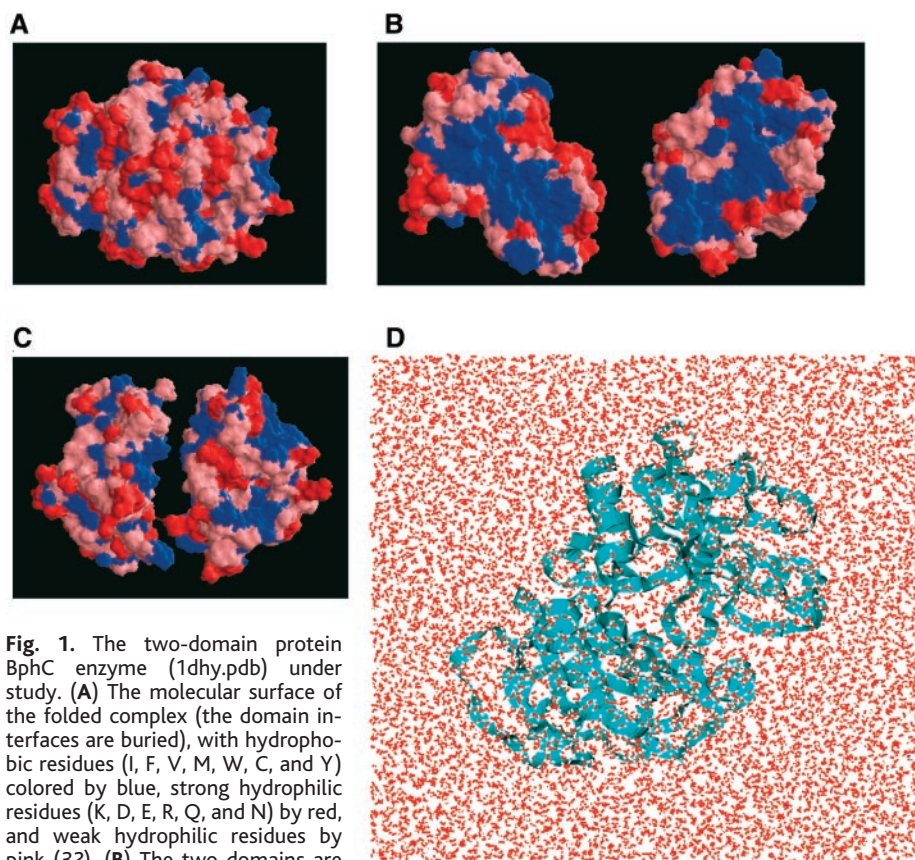


Fig. 1. The two-domain protein BphC enzyme (1dhy.pdb) under study. (A) The molecular surface of the folded complex (the domain interfaces are buried), with hydrophobic residues (I, F, V, M, W, C, and Y) colored by blue, strong hydrophilic residues (K, D, E, R, Q, and N) by red, and weak hydrophilic residues by pink (32). (B) The two domains are separated and rotated such that the interface areas are facing the reader. Large hydrophobic surface areas can be seen on the domain boundary. (C) The two domains are separated along the line of the two domain centers so that the interface can be seen. (D) Solvated protein system in water, with the interdomain gap distance $D = 6 \text{ \AA}$.

tion gives rise to a vapor layer a few water molecules thick (1, 2), each domain is solvated in water alone and a 2-ns NPT simulation is run after a normal 100-ps equilibration. No meaningful vapor layer was found in either of the two single domains of BphC. This result is not unexpected, because the electrostatic and dispersion attractions in the protein-water interactions should not only “pull” the water interface closer to the surface of the protein but also damp out the capillarity waves, two effects contributing to the disappearance of a vapor layer.

To investigate the time scale and kinetics for dewetting in the hydrophobic collapse of BphC, we initially set the interdomain gap distance $D = 6$ Å. In a 5-ns NPT simulation, D consistently decreases as water molecules leave the intervening region. After about 1.5 ns, the decrease slows because the final residual water molecules are becoming harder to expel. Some of them are deeply buried in the hydrophobic cavities between the two domains, which makes them more difficult to escape because most possible escape pathways are blocked. After about 5 ns, only a few water molecules are still left in the interdomain region. During the entire 5-ns folding simulation, the two individual domains stay folded, with backbone root mean square displacement from the starting native structures less than 2.0 to 2.5 Å and the fluctuations in the radius of gyration less than 0.5 Å for each domain. The dynamics of the interdomain collapse are shown in Fig. 3B. The two domains approach each other faster in the first nanosecond and then slow down considerably when D decreases to about 1.2 Å. Consistent with the dewetting

and wetting simulations discussed above, no SDT is observed.

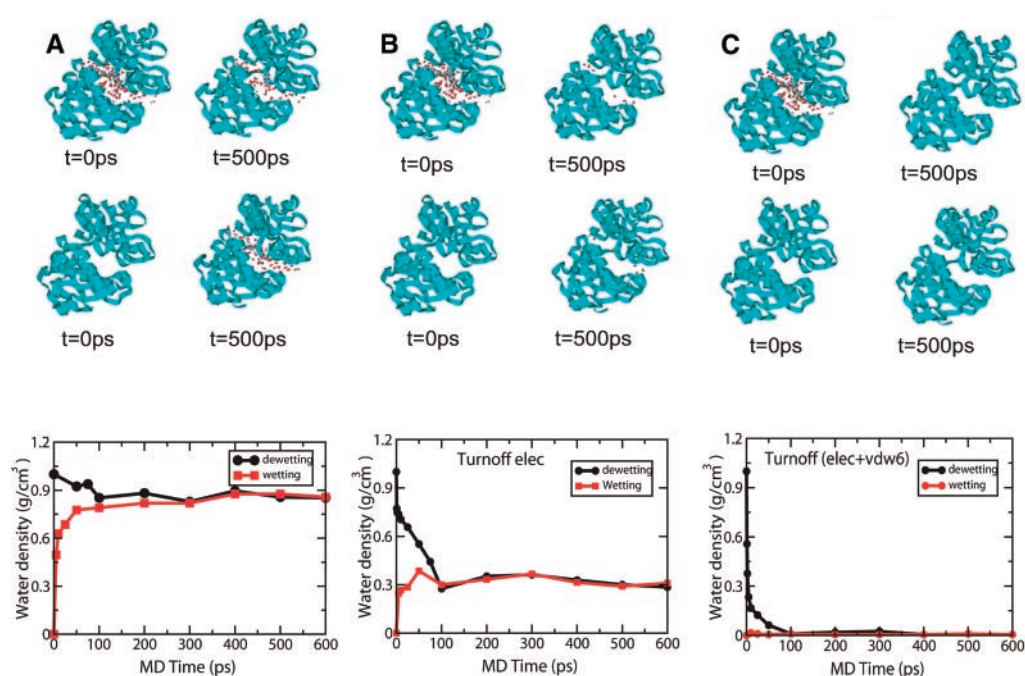
The collapse of BphC is much different from the collapse of idealized paraffin-like plates (3). The observed kinetics of hydrophobic collapse of two hydrophobic plates is characterized by two temporal regimes (Fig. 3A). Initially, the distant plates diffuse toward each other, with water filling the region between them, until they reach a critical separation; then a drying transition takes place that is equivalent to a liquid-gas phase transition of the confined liquid. The two plates are then driven quickly together, so there are two kinetic regimes. The equivalent collapse of the two-domain protein BphC enzyme (Fig. 3B) showed no two-speed collapse, and the actual speed is two orders of magnitude slower than that found in the idealized paraffin-like plates.

Why do these two systems behave so differently? To better understand the observed differences in the dewetting and collapse of idealized paraffin-like plates and of the two-domain protein, we turn off different parts of the protein-water and domain-domain interactions. We designate three different ways for turning interactions off. In “Turnoff1,” we turn off protein-water electrostatic interactions. In “Turnoff2,” we also turn off protein-water van der Waals attractions (r^{-6} term). In “Turnoff3,” we additionally turn off domain-domain electrostatic and van der Waals attractive interactions. The snapshots for dewetting and wetting simulations are shown in Fig. 2 for both Turnoff1 (Fig. 2B) and Turnoff2 (Fig. 2C). (Because domains are constrained in space in both dewetting and wetting simulations, the Turn-

off3 option does not apply here.) The water density drops (Fig. 2B, bottom) to approximately 0.3 g cm^{-3} in the Turnoff1 case. These remaining water molecules are at the edge of the interdomain gap region, leaving the center area empty. The water density drops further to essentially zero in the Turnoff2 case (Fig. 2C, bottom). Thus, for these last two cases, an SDT is found, even though the protein domain surfaces are rough (30). A dewetting critical distance (3) of 7 to 9 Å and 18 to 20 Å are found, respectively, for the Turnoff1 and Turnoff2 cases. The critical distance increases greatly when the protein-water van der Waals attraction is turned off. The critical distance for the Turnoff2 case agrees very well with the results for the idealized paraffin-like plates (3), which indicates that the extent of dewetting in Turnoff2 resembles that of the hydrophobic plates despite its rough hydrophobic surfaces.

The water depletion around isolated single domains is also very sensitive to turning off parts of the interaction (31). With the full potential, no depletion was observed. With protein-water electrostatic interactions turned off (Turnoff1), the water depletion extends to 5 to 6 Å, with an average water density approximately 10% lower than the bulk. With the van der Waals attractions also turned off (Turnoff2), the water depletion extends to about 8 Å, with an average water density approximately 30% lower than the bulk. Interestingly, two recent experiments (6, 9, 10) have also found about a 10% water density decrease near hydrophobic surfaces. Steitz *et al.* (9), studying D_2O in contact with deuterated polystyrene in neutron reflectivity experiments, found a 6 to 12% density decrease in

Fig. 2. (A) Snapshots of water configurations inside the domain gap region started from both the initial wet condition (top) and the initial dry condition (middle) for $D = 4$ Å. (To provide a better view, only the water molecules inside the gap region are shown.) The corresponding water densities inside the gap region are also shown for both cases versus time (bottom). This is for a simulation with full force-field interactions. (B) Same as (A), except that the protein-water electrostatic interactions are turned off. (C) Same as (A), except that both the protein-water electrostatic interactions and the van der Waals attractive interactions are turned off.



a depletion layer of roughly 20 Å. Jensen *et al.* (10) used x-ray reflectivity to study water in contact with paraffin and found a 10% density decrease in a depletion layer of no more than 15 Å. Thus, the water depletion for Turnoff1 is similar to the results found in these experiments but does not extend as far out from the hydrophobic surface. The reorganization of water around simple but sufficiently large hydrophobic solutes with concomitant depletion was also anticipated theoretically (1, 2, 4).

The folding kinetics for different turnoff schemes are shown in Fig. 3C. The snapshots of protein-water configurations are shown only for the Turnoff2 case, whereas the time evolution of *D* is shown for all three cases. The folding (and drying) time decreases by a factor of 10 in Turnoff1, from about 1500 ps

to 150 ps. It further decreases to about 25 ps in Turnoff2, which is comparable to the time scale in idealized paraffin-like plate collapse. Interestingly, Turnoff3 increases the drying time slightly compared with Turnoff2 because of the net van der Waals (r^{-12}) repulsion between the two domains (note the slightly larger equilibrated gap distance), but both are comparable to the idealized hydrophobic plates. This much faster speed can also be seen from the time scales required to reach equilibrium in the dewetting and wetting simulations in Fig. 2. These results indicate that turning off protein-water electrostatic interactions can dramatically speed up the drying kinetics, which is further accelerated by turning off the van der Waals attractions. Thus, by removing the protein-water attractive interactions, the dewetting and collapse

resemble what was previously seen in idealized paraffin-like plates, with respect to both the extent of dewetting and the speed of hydrophobic collapse, despite the protein's having much rougher hydrophobic surfaces than the idealized plates. We found that the kinetics of collapse is more affected by the electrostatic interactions, whereas the critical distance D_c of dewetting is more affected by the van der Waals attractions.

Finally, as mentioned above, for idealized paraffin-like plates that do not attract each other or water, the plates diffuse toward each other until they reach a critical separation, upon which a large-scale drying transition takes place, followed by a rapid collapse, i.e., a two-speed-like collapse. However, even in the collapse of the two domains in Turnoff3, which supposedly mimics the idealized plates, we do not observe this two-speed-like collapse, partly because the two protein domains have a linker (loop) between them that constrains the speed at which the domains can collapse even in the absence of water and also limits the pathways through which water can flow.

One lesson learned from our simulations is that models found useful for describing the dewetting and collapse of aggregation of oil drop-like particles, although useful for understanding the collapse of simple hydrophobes, cannot, in their present form, account for the behavior observed in the simulation of the collapse of BphC. These simple models would predict that as the two domains approach each other, when they get closer than some critical distance, there would be a sudden drying transition in the interdomain region (much like what would happen in a gas-liquid phase transition), followed by a rapid collapse of the two domains. This behavior is not seen in our two-domain protein, and we believe that it will not be seen in other multidomain proteins either. We find that the degree of dewetting depends critically on the strength of the solute-solvent electrostatic interactions, which apparently are large enough in proteins to make the simple models of hydrophobic dewetting and collapse inapplicable in their present form. It is of considerable interest to devise experiments to test our above predictions for multidomain proteins or protein aggregates.

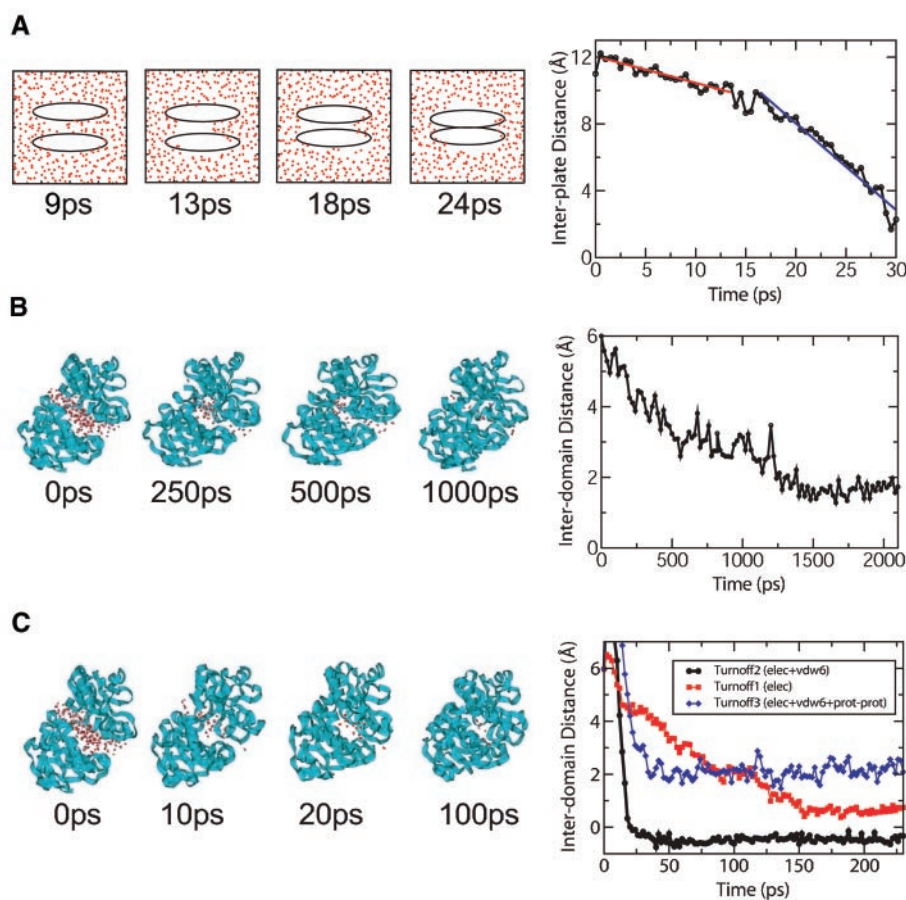


Fig. 3. Comparison of the kinetics of hydrophobic collapse for the idealized plates and the two-domain protein, with or without part of the interactions turned off. (A) Snapshots of the hydrophobic collapse of the two plates (left) and the distance between two plate centers versus time (right). (B) Snapshots of the folding of the two-domain protein with full interactions (left) and its gap distance versus time (right). (C) Same as (B) but with various interactions turned off. The snapshots (left) are for the case in which the protein-water electrostatic and van der Waals attractions are turned off (Turnoff2). The distance curves (right) show three different options: red for Turnoff1 (only protein-water electrostatic interactions are turned off); black for Turnoff2 (Turnoff1 plus turning off the protein-water van der Waals attractive interactions); and blue for Turnoff3 (Turnoff2 plus turning off the domain-domain electrostatic and van der Waals attractive interactions). These figures show a very fast collapse of the hydrophobic plates and a very slow (orders of magnitude slower) two-domain protein folding. However, with part of the attractive interactions turned off, the protein domains collapse on a much faster time scale, just like the idealized plates.

References and Notes

1. K. Lum, D. Chandler, J. D. Weeks, *J. Phys. Chem. B* **103**, 4570 (1999).
2. D. M. Huang, D. Chandler, *J. Phys. Chem. B* **106**, 2047 (2002).
3. X. Huang, C. J. Margulis, B. J. Berne, *Proc. Natl. Acad. Sci. U.S.A.* **100**, 11953 (2003).
4. F. H. Stillinger, *J. Solution Chem.* **2**, 141 (1973).
5. D. Chandler, *Nature* **417**, 491 (2002).
6. P. Ball, *Nature* **423**, 25 (2003).
7. C. Pangali, M. Rao, B. J. Berne, *J. Chem. Phys.* **71**, 2982 (1979).
8. G. Hummer, J. C. Rasaiah, J. P. Noworyta, *Nature* **414**, 188 (2001).

9. R. Steitz *et al.*, *Langmuir* **19**, 2409 (2003).
10. T. R. Jensen *et al.*, *Phys. Rev. Lett.* **90**(8), 86101 (2003).
11. A. Wallqvist, B. J. Berne, *J. Phys. Chem.* **99**, 2893 (1995).
12. A. Wallqvist, B. J. Berne, *J. Phys. Chem.* **99**, 2885 (1995).
13. K. Leung, A. Luzar, *J. Chem. Phys.* **113**, 5845 (2000).
14. K. Leung, A. Luzar, D. Bratko, *Phys. Rev. Lett.* **90**, 65502 (2003).
15. M. E. Paulaitis, L. R. Pratt, *Adv. Protein Chem.* **62**, 283 (2002).
16. L. R. Pratt, *Annu. Rev. Phys. Chem.* **53**, 409 (2002).
17. G. Hummer, S. Garde, A. E. Garcia, L. R. Pratt, *Chem. Phys.* **258**, 349 (2000).
18. K. Lum, A. Luzar, *Phys. Rev. E.* **56**, R6283 (1997).
19. D. M. Huang, D. Chandler, *Proc. Natl. Acad. Sci. U.S.A.* **97**, 8324 (2000).
20. P. R. ten Wolde, D. Chandler, *Proc. Natl. Acad. Sci. U.S.A.* **99**, 6539 (2002).
21. K. Lum, D. Chandler, *Int. J. Thermophys.* **19**, 845 (1998).
22. R. D. Mountain, D. Thirumalai, *J. Am. Chem. Soc.* **125**, 1950 (2003).
23. R. Zhou, B. D. Silverman, A. Royyuru, P. Athma, *Proteins* **52**, 561 (2003).
24. The starting structure is taken from the crystal structure deposited in PDB (entry 1dhy.pdb). The interdomain distance of the crystal structure is increased by D along the direction of two domain centers of geometry to create "gaps" between the two domains (to make room for water). Various distances ranging from $D = 2.5 \text{ \AA}$ to 20.0 \AA are studied. The resulting protein configurations are then solvated in a water box, with water layers at least 8 \AA from the protein surfaces. Figure 1 shows one such solvated configuration. Eight Na^+ counterions are added to make the system electrically neutral. The solvated protein systems have up to 42,000 atoms (the actual size varies for different interdomain distances). The GROMACS simulation package is used here for this large system because of its fast speed (25). Each NPT MD simulation [(26), 1 atm and 300 K] is run in parallel with 8 to 16 processors on IBM SP2-Power3-375 MHz clusters. The OPLSAA force field is used for the protein (27), and a simple point charge (SPC) water model is used for the explicit solvent. For the long-range electrostatic interactions, the particle-mesh Ewald method is used. For the van der Waals interactions, a typical 10 \AA cutoff is used. A time step of 2.0 fs is used with bond lengths constrained. A standard equilibration procedure, which includes a conjugate gradient minimization and a 100-ps MD simulation with position restraints, is followed to equilibrate each solvated system. The final configurations from equilibration are then used for data collection. We have modified GROMACS to allow us to selectively turn off certain terms in the force field, in particular, the protein-water electrostatic potential, the attractive part of the protein-water van der Waals potential, the domain-domain electrostatic potential, and the attractive part of the domain-domain van der Waals potential. This approach allows us to make a sensitivity analysis of hydrophobic collapse and to compare the protein collapse with what is already known about the hydrophobic collapse of the plates.
25. E. Lindahl, B. Hess, D. van der Spoel, *J. Mol. Model.* **7**, 306 (2001).
26. One caveat is that NPT MD introduces fictitious dynamics from both the temperature and pressure control. New fictitious degrees of freedom are introduced, with corresponding kinetic energies, fictitious masses, and fictitious frequencies. These influence the time scales and can affect the rate processes observed. Nevertheless, the thermodynamic equilibrium water densities inside the interplate or interdomain region and the water depletion or dewetting phenomena should stay the same. Our observations about kinetics are borne out in careful studies.
27. W. L. Jorgensen, D. Maxwell, J. Tirado-Rives, *J. Am. Chem. Soc.* **118**, 11225 (1996).
28. The original total interdomain distance is about 18.8 \AA , so after the enlargement, the total interdomain distance is about 22.8 \AA . For simplicity, we will refer to it as interdomain gap distance $D = 4 \text{ \AA}$ in the following.
29. It is tricky to define the water density inside the domain gap region, particularly for cases with very small D values, because the fluctuation in the number of water molecules can be fairly large compared with the total number of water molecules inside the region. In general, it is very difficult to directly measure the volume inside the domain gap region because of the irregularity of the protein domain structures; thus, we used a comparative way to measure the water density.
30. Y. Cheng, P. J. Rossky, *Nature* **392**, 696 (1998).
31. H. S. Ashbaugh, M. E. Paulaitis, *J. Am. Chem. Soc.* **123**, 10721 (2001).
32. Single-letter abbreviations for the amino acid residues are as follows: A, Ala; C, Cys; D, Asp; E, Glu; F, Phe; G, Gly; H, His; I, Ile; K, Lys; L, Leu; M, Met; N, Asn; P, Pro; Q, Gln; R, Arg; S, Ser; T, Thr; V, Val; W, Trp; and Y, Tyr.
33. This work was partially supported by a grant to B.J.B. from NIH (GM4330) and a Shared University Research (SUR) grant from the IBM Corporation to Columbia University.

7 June 2004; accepted 20 August 2004

Climate Impact on Plankton Ecosystems in the Northeast Atlantic

Anthony J. Richardson^{1*} and David S. Schoeman²

It is now widely accepted that global warming is occurring, yet its effects on the world's largest ecosystem, the marine pelagic realm, are largely unknown. We show that sea surface warming in the Northeast Atlantic is accompanied by increasing phytoplankton abundance in cooler regions and decreasing phytoplankton abundance in warmer regions. This impact propagates up the food web (bottom-up control) through copepod herbivores to zooplankton carnivores because of tight trophic coupling. Future warming is therefore likely to alter the spatial distribution of primary and secondary pelagic production, affecting ecosystem services and placing additional stress on already-depleted fish and mammal populations.

Not only do plankton provide food for marine mammals and commercially important fish, they also play a fundamental role in the functioning of marine ecosystems by providing half the global primary production (1) and contributing substantially to biogeochemical cycling (2). How global climate change might affect biological communities such as marine plankton is therefore a matter for concern (3). There is evidence of climate-mediated biogeographical shifts among some groups of marine plankton such as the calanoid copepods (4), but the overall response of phytoplankton and zooplankton communities, which is likely to depend on the form and strength of the linkages between successive trophic levels, is not known. Until we understand these processes, we will not know how resilient such food webs are to global-scale impacts, such as climate change, eutrophication, pollution, or over-fishing, and it will be difficult to manage marine resources sustainably.

To predict the response of the base of the marine food web to climate change, we need a better understanding of the type and degree

of coupling between trophic levels in marine systems. Complex biological systems are generally controlled by their top predators through top-down control, by their producers through bottom-up control, or by a number of key species in the middle through wasp-waist control (5). For the plankton ecosystem within the marine pelagic realm, there is currently conflicting evidence on when these types of control operate, and on what scales. Some workers suggest tight bottom-up coupling of plankton trophic levels (2, 6, 7), whereas others conclude that strong top-down control (8) or weak coupling (9, 10) is operative.

Complicating the identification of processes underpinning marine food web dynamics is a range of methodological limitations: time series of biotic variables tend to be short; spatial coverage of most studies is restricted to point sampling; and syntheses often attempt to combine results from studies with very different field and analytical approaches. We overcome such problems by using 115,322 samples taken by the Continuous Plankton Recorder (CPR) survey in the Northeast Atlantic between 1958 and 2002. These samples have been collected, processed, and analyzed in a consistent manner, yielding reliable time series for ~400 taxa (11) and providing a unique opportunity to investigate planktonic ecology over decadal and ocean basin scales. Using these data, we construct a conceptual pelagic food web

¹Sir Alister Hardy Foundation for Ocean Science, The Laboratory, Citadel Hill, Plymouth, PL1 2PB, UK. ²Department of Zoology, University of Port Elizabeth, Port Elizabeth, South Africa.

*To whom correspondence should be addressed. E-mail: anr@sahfos.ac.uk